HIGH-ENERGY MUON-PAIR PRODUCTION AND THE DRELL-YAN MODEL*

By F. Vannucci

Laboratoire de Physique des Particules (LAPP), Annecy**

(Received August 19, 1980)

New results from some high statistics experiments measuring muon-pair production in proton- and pion-induced reactions are discussed.

PACS numbers: 13.85.—t, 13.85.Hd

1. Introduction

New results from several high statistics experiments measuring muon-pair production in proton- and pion-induced reactions are now available. In particular several experiments done at CERN, both at the Intersecting Storage Rings (ISR) and the Super Proton Synchrotron (SPS), enlarge the kinematical domain investigated before. With these new results the emphasis of the interpretation, which was not long ago on proving qualitatively the annihilation mechanism of the Drell–Yan model, is now on quantifying the disagreements between the naïve model and the experimental results. Of special interest is the study of the dimuon transverse momentum and of the extraction of structure functions for which higher-order diagrams in QCD seem to be required.

2. Dimuon experiments

2.1. General considerations

Why do we study dilepton physics? Because the J/ψ and the Υ were discovered in the dilepton decay mode and because electrons and muons have properties characteristic enough to allow extraction from an overwhelming hadronic background. More recently the interest has also been on the continuum which gives information on the parton distributions inside the nucleon.

---

* Presented at the XX Cracow School of Theoretical Physics, Zakopane, May 29 — June 11, 1980.

** Address: LAPP, Chemin de Bellevue, B.P. 909, 74019 Annecy-le-Vieux Cedex, France.

And why do we use muons instead of electrons? Because production rates are much smaller than in hadronic processes one wants the highest possible beam intensity in order to accumulate large statistics. Electrons need open detectors; on the contrary muons are identified after an absorber which shields the detector against hadrons. Backgrounds in such experiments come from hadron punch-through and π and K decays emitting a muon. These backgrounds are minimized by using an absorber of many collision lengths, which starts as close as possible to the interaction vertex. The momentum analysis of the muons can be done before, after, or inside the absorber, with all possible mixed solutions.

Results which will be discussed essentially come from the following experiments:

(*i*) In proton-induced reactions the experiments are those of the Columbia–FNAL–Stony Brook (CFS) Collaboration [1] and the CERN–Harvard–LAPP–MIT–Naples–Pisa Collaboration [2] at the ISR.

(*ii*) In pion-induced reactions, the experiments are those of the Chicago–Princeton (CP) Collaboration [3], the CERN–Collége de France–Ecole Polytechnique–Orsay–Saclay Collaboration (NA3) [4], and the Saclay–Imperial College–Southampton–Bloomington Collaboration (WA11) [5].

2.2. The dimuon experiment at the ISR [2]

The special difficulty of this experiment comes from the fact that the reaction takes place almost in the centre of mass of the two incident protons. One has to cover a large solid angle to catch a good fraction of the produced dimuons. Magnetized iron is the

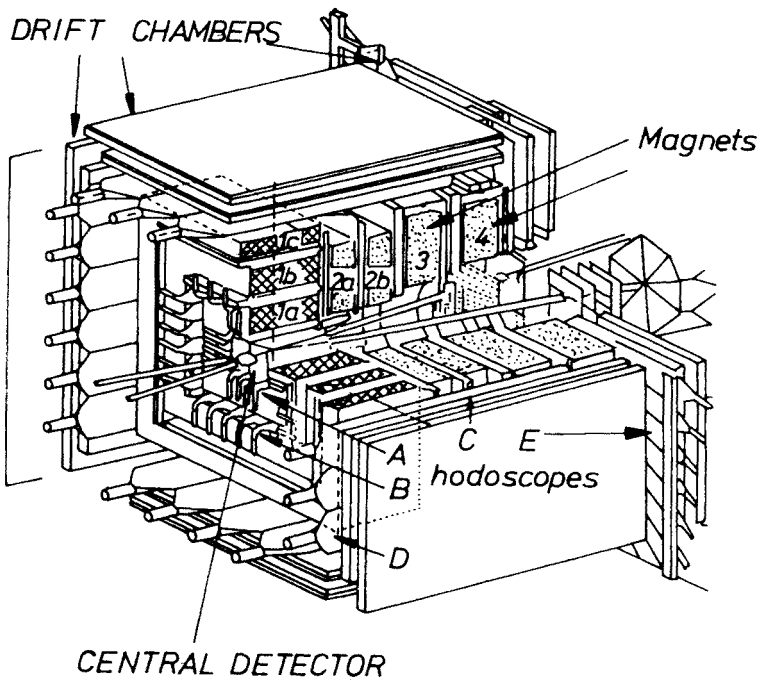

Fig. 1. Dimuon spectrometer of the CHMNP experiment at the ISR

cheapest way of filling a large volume with a high magnetic field (1.8 T). At the same time, it provides a filter to absorb hadrons.

The detector is shown in Fig. 1. It consists of 500 t of large toroids of magnetized iron giving a minimum $B\,dl$ of 2.7 T · m over a solid angle of 8 sr. The iron is sandwiched between large drift chambers giving a spatial resolution of 0.7 mm over a total area of 800 m^2. Large hodoscopes of scintillator counters are used to trigger and also to reject background cosmic-rays and stray particles by the time-of-flight technique.

The minimum thickness of iron in the path of a particle is 1.5 m and the absorber starts 50 cm from the interaction. This technique proves effective: about 10^7 charged particles are produced every second, but the trigger rate is only 0.5 per second for a typical luminosity of 10^{31} cm^{-2} s^{-1}.

The inner hole of the first yoke directly surrounding the interaction point is filled with drift wire and delay-line chambers, which help reconstruct the vertex and give information on the hadrons produced together with the muon pair.

Figure 2 shows the resulting plot of dimuon masses obtained at the c.m. energy $\sqrt{s}$ = 62 GeV. This plot is based on an integrated luminosity of 1.11×10^{38} cm^{-2}. There

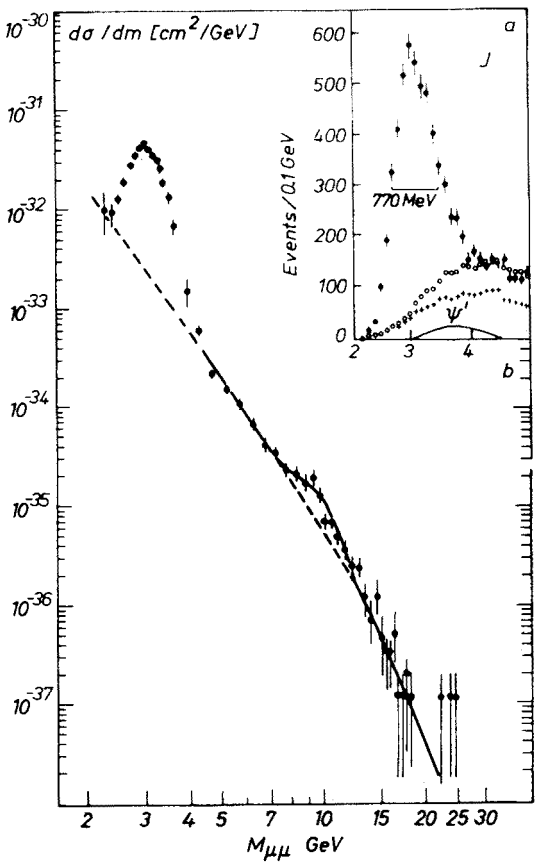

Fig. 2. Dimuon mass spectrum from the CHMNP experiment

are events up to and beyond 20 GeV of mass. The background level is checked by the amount of like-sign pairs: it is negligible above a mass of 7 GeV/c^2.

Compared with a stationary target experiment, the ISR experiment loses a large factor in luminosity, but the ISR remains the highest energy machine and this is important for tests of scaling. Furthermore, as will be seen, the ISR experiment measures the continuum is a region of τ inaccessible to the FNAL/SPS experiments. Finally, the low luminosity ceases to be a handicap for the study of associated hadrons, for which virtually no information is yet available.

3. The Drell–Yan model [6]

3.1. The naïve model

In this model the massive-lepton-pair production

$$A+B \to l^+ + l^- + X$$

takes place via the annihilation of a quark of one incoming hadron with an antiquark of the other hadron into a time-like photon. The photon then decays into a lepton pair, as shown in Fig. 3, where kinematical variables are defined.

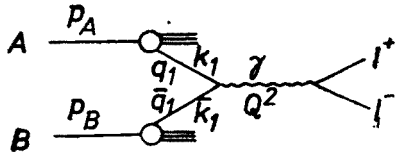

Fig. 3. Diagram of the Drell–Yan process

The cross-section is obtained by summing incoherently over the elementary processes $q_i+\bar{q}_i \to l^+ + l^-$, weighted by the probability of finding quarks and antiquarks which will annihilate with each other:

$$(A+B \to l^+ + l^- + X) = \iiint dx_1 dx_2 \sum_i [f_i^A(x_1)\bar{f}_i^B(x_2)+\bar{f}_i^A(x_1)f_i^B(x_2)]$$

$$\times \sigma(q_i\bar{q}_i \to l^+l^-)\delta[q^2-(k_i+\bar{k}_i)^2]dq^2,$$

where x_1 and x_2 refer to hadrons A and B respectively.

In the simple model quarks have small intrinsic transverse momentum k_T and the probability functions f, $\bar{f}$ only depend on the dimensionless quantities x_1, x_2 which are the fraction of initial momentum carried by the constituents:

$$k_i = x_1^i P_A, \quad \bar{k}_i = x_2^i P_B.$$

The two directly measurable parameters are:

(*i*) the scaled mass squared: $\tau = m^2/s$. In the limit of large c.m. energy $s = (P_A+P_B)^2$, $\tau \simeq x_1 x_2$;

(*ii*) the Feynmann variable: $x_F = 2P_L/\sqrt{s} = x_1 - x_2$.

Assuming a point-like coupling, $\gamma q_i \bar{q}_i$, one finds the cross-section:

$$m^3 \frac{d^2\sigma}{dm dx_F} = \frac{8\pi\alpha^2}{3N_c} \frac{1}{\sqrt{x_F^2+4\tau}} \sum_i e_i^2 [f_i^A(x_1)\bar{f}_i^B(x_2) + \bar{f}_i^A(x_1) f_i^B(x_2)],$$

e_i being the charge of the quark of type i. Notice that the $f(x)$ are now the structure functions defined by x (probability distributions).

The predictions of the model are as follows:

a) The cross-section should scale: $m^3 d\sigma/dm$ and $m^3 d^2\sigma/dm dx$ are universal functions of the dimensionless variable τ and do not depend on energy.

b) The cross-section is inversely proportional to the number of colours N_c.

c) Quarks having spin $\frac{1}{2}$ and point-like coupling to the photon, the angular distribution of one lepton in the dilepton c.m. system is $1+\cos^2\theta$.

d) The cross-section is determined in shape and amplitude by the quark distribution functions extracted in deep inelastic lepton scattering experiments.

e) k_T being small, the transverse momentum p_T of the dilepton should be small.

f) Finally one expects two jets, fragments of the initial hadrons accompanying the lepton pair.

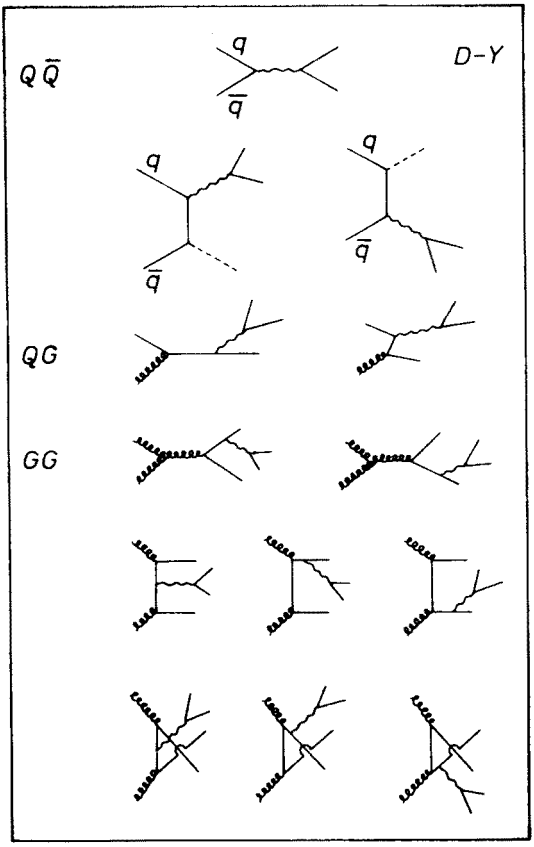

Fig. 4. Higher-order diagrams

3.2. The educated model [7]

There are two reasons to go beyond the naïve model: the known scaling violation in deep inelastic scattering which requires a q^2 dependence of the structure functions; and the large p_T found in dimuon experiments, contrary to expectations.

There are also theoretical reasons to go beyond the only annihilation graph. Higher-order graphs cannot be dismissed. For example, graphs of order α_s and α_s^2 are shown in Fig. 4. They give contributions $\alpha_s \log Q^2$ and $(\alpha_s \log Q^2)^2$, respectively. Quantum Chromodynamics (QCD) tells us that $\alpha_s \propto 1/\log Q^2$ and one sees that these terms and even higher-order terms are not negligible.

The simple model has to be refined at two levels:

(*i*) In the leading log approximation, the cross-section integrated over p_T is still valid as long as one replaces $f(x)$ by the no longer scaling $f(x, q^2)$ extracted from deep inelastic scattering experiments.

(*ii*) Beyond these modifications one still expects QCD corrections proportional to $1/\log Q^2$. In the range of τ experimentally measured these corrections are roughly constant [8]. This means that they affect the over-all normalization and can be as large as 100%.

4. Manifestations of $q\bar{q}$ annihilation

4.1. Target dependence

The Drell-Yan process postulates an incoherent action of the different scatterers inside the nucleon. The total cross-section can be expected to vary linearly with A, the atomic number of the target. This is different with hadronic processes which vary as $A^{2/3}$.

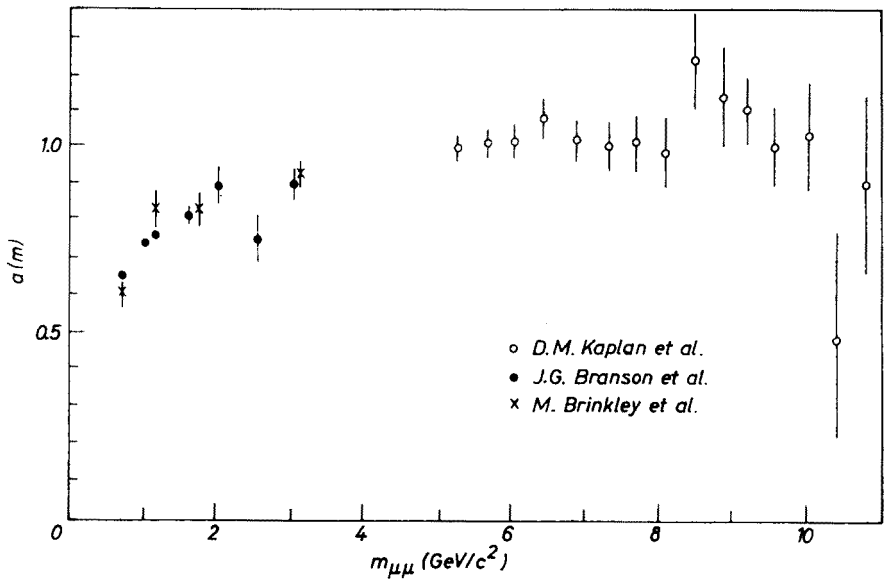

Fig. 5. A dependence of the dimuon cross-sections

Figure 5 shows the A dependence as a function of the dimuon mass $m_{\mu\mu}$, in the case of a proton beam. Data come from Refs. [1] and [9]. There is a clear transition occurring at a mass $\sim$4 GeV from a possible $A^{2/3}$ to an A dependence, indicative of a change of régime for dimuon production. In pion reactions, the CP experiment found an exponent $\alpha = 1.12 \pm 0.05$ above 4 GeV mass, but the recent result from NA3 supports the idea of incoherent parton interactions with $\alpha = 1.03 \pm 0.03$. This difference causes some difficulty in comparing these two experiments.

4.2. Beam dependence

The annihilation occurs between a quark of one hadron and an antiquark of the second hadron. The target consists of protons and neutrons for which antiquarks exist only in the sea. The projectile quark distribution offers more variety and one expects the following relations:

$$\sigma(\bar{p}p) > \sigma(\bar{n}p) > \sigma(pp) > \sigma(np),$$

$$\sigma(\pi^- p) = \sigma(K^- p) > \sigma(\pi^+ p) = \sigma(\bar{K}^0 p) > \sigma(K^+ p) = \sigma(K^0 p).$$

Good data from the NA3 experiment exist now with π^+, π^-, K^+, K^-, p, and $\bar{p}$ beams. Figure 6 shows the mass spectra obtained with 200 GeV π^+, π^-, K^+, and K^- beams, normalized to the same incident particle flux. The results are compatible not only with $\sigma(\pi^- p) = \sigma(K^- p)$ but also with $\sigma(\pi^+ p) = \sigma(K^+ p)$. For the comparison between $\sigma(\pi^- p)$ and $\sigma(\pi^+ p)$,

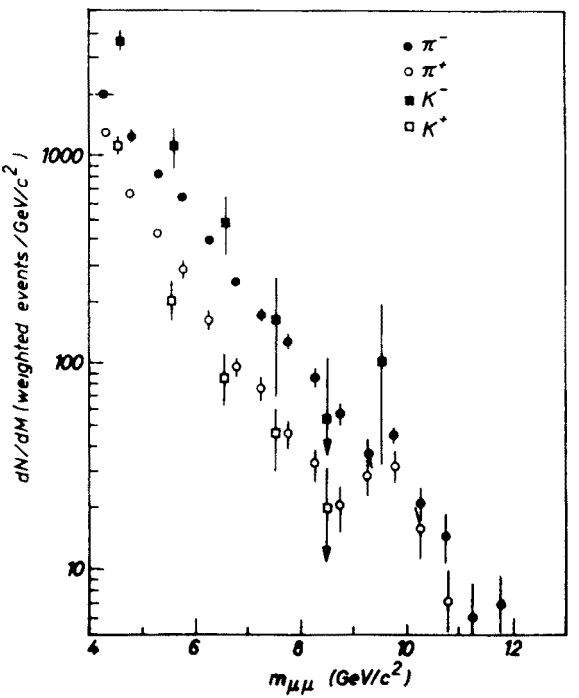

Fig. 6. Production cross-sections with π^+, π^-, K^+, and K^- beams

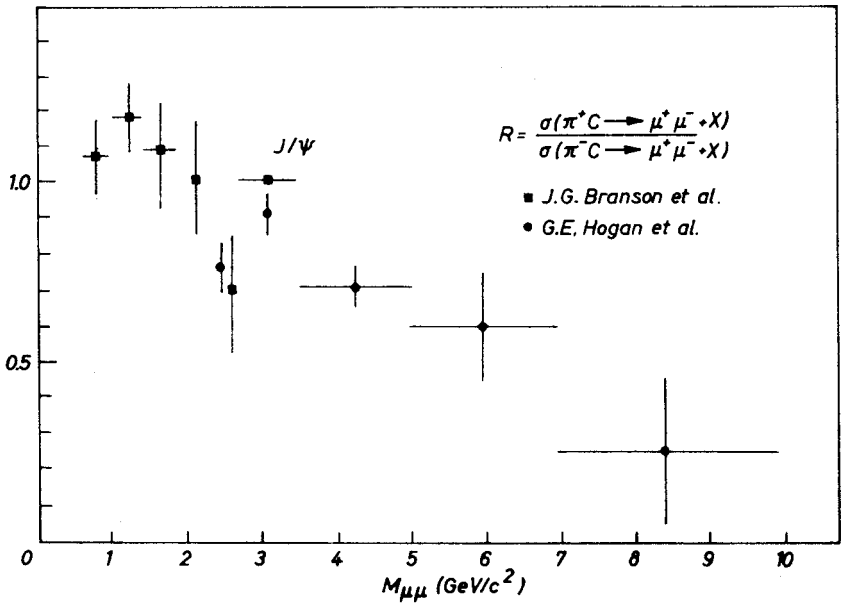

Fig. 7. Ratio of productions with π^+ and π^- beams

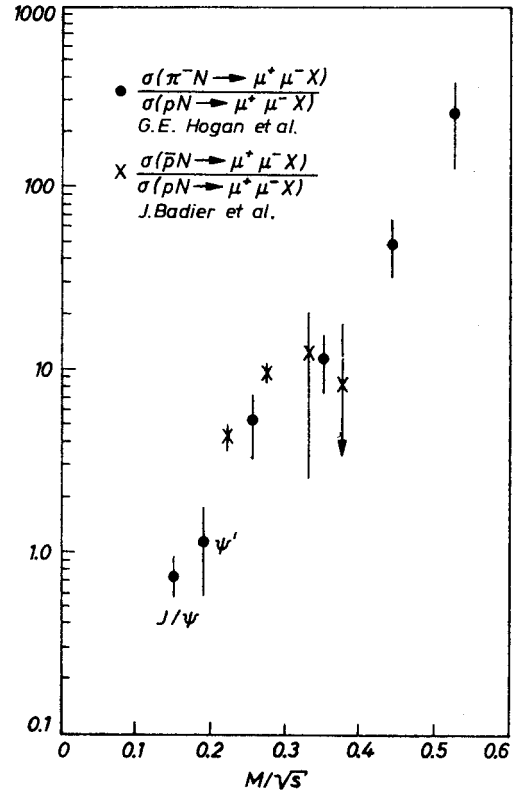

Fig. 8. Ratios of production π^-/p and $\bar{p}/p$

the prediction on an isoscalar target is:

$$\frac{\sigma(\pi^+ N)}{\sigma(\pi^- N)} = \frac{e_d^2 d(x)\bar{d}(x)}{e_u^2 u(x)\bar{u}(x)} = \frac{1}{4}.$$

This is true in the limit of no sea-quark contamination. Figure 7 shows the experimental results obtained with a carbon target. There is indeed a transition from a ratio 1 expected for hadronic production to a ratio compatible with 0.25 at high dimuon mass.

The result for $\sigma(\pi^- N)/\sigma(pN)$ is even more remarkable, as shown in Fig. 8. The ratio equal to 1 at low mass reaches 200 for a 10 GeV mass. This is easily explained by the existence of valence antiquarks in the π^-, while p has only sea antiquarks carrying less momentum. The ideal test of this idea is the comparison between $\sigma(\bar{p}N)$ and $\sigma(pN)$. The ratio is also displayed in Fig. 8.

Higher statistics results will soon be available, allowing for more refined tests, for instance sum rules based on simple charge counting like:

$$\sigma(\pi^- p) - \sigma(K^+ p) = 4[\sigma(\pi^+ n) - \sigma(K^+ n)].$$

4.3. Angular distribution

In the simple annihilation mechanism, the angular distribution of one lepton in the dimuon system is predicted to be:

$$\frac{d\sigma}{d\Omega} = A(1+\cos^2\theta).$$

θ is measured from the $q\bar{q}$ direction; if quarks have no transverse momentum the initial hadrons define this direction.

Results exist in pion production from the CP and NA3 experiments and in proton production from the ISR experiment. The distribution is compatible, in both cases, with a $1+\cos^2\theta$ dependence outside the resonances, while it is flatter at the J/ψ and also at the γ. This gives good evidence for spin alignment of the annihilating constituents.

Beyond the simple Drell–Yan model it is predicted that, at large x, the intermediate photon can get a longitudinal polarization [10], thus giving a distribution which should vary as $\sin^2\theta$. Recent results from the CP experiment support this idea.

5. Test of scaling

The scaling law $m^3 d\sigma/dm = F(\tau)$ is a basic prediction of the Drell–Yan model. It also simply follows from dimensional analyses. It implies that the quark distribution functions depend only on the dimensionless variable x. Scaling violations, on the contrary, could be generated by some quark form factors dependent on q^2.

Scaling violations have been seen in deep inelastic experiments, but the recent data

on neutrino [11] and muon [12] deep scattering show that scaling violations are only important for small q^2 ($q^2 < 20\ \mathrm{GeV}^2$) and large x ($x > 0.4$). There has been, up to now, no experimental evidence of sizeable scaling violation for processes with $q^2 > 20\ \mathrm{GeV}^2$.

5.1. Scaling in π production

The WA11 experiment has checked scaling between cross-sections obtained for 150 and 175 GeV incident beams. The NA3 experiment has done likewise for 200 and 280 GeV beams. Figure 9 shows the quantity $m^3 d\sigma/dm$ plotted as a function of $\sqrt{\tau} = m/\sqrt{s}$ for 150, 225, and 280 GeV π beams. These three curves come from three different experiments: WA11, CP, and NA3, respectively. The agreement between the two extreme beam energies is relatively good. Comparing spectra obtained at different energies in the same detector does not test scaling within better than 20% accuracy. One should not be surprised that any comparison of different experiments with different systematic errors gives a test valid at the 50% level. The discrepancy between the CP result, obtained at an intermediate energy,

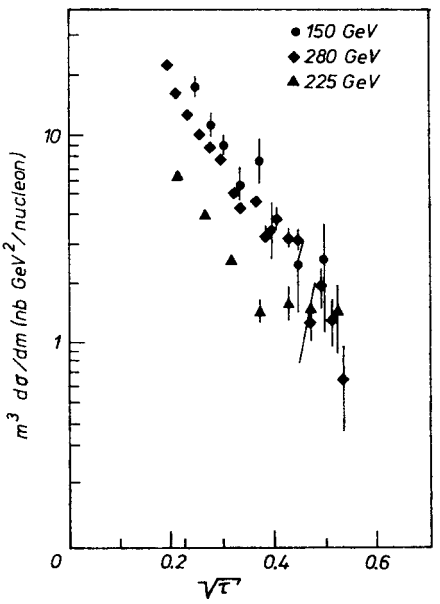

Fig. 9. Scaling in π^--induced reactions

and the two other results seems to be a reflection of the different exponent in the A dependence of the cross-section. It is interesting to note that taking A^1 for all three experiments restores scaling, while taking $A^{1.12}$ for all experiments keeps an apparent scaling violation.

In passing one may note that such a test is not very compelling because of the very limited kinematical range explored: $\sqrt{s}$ varies from 17.3 to 23.7 GeV. This means that the overlap region extends in q^2 from 15 to 28 GeV^2 at $\tau = 0.05$ and from 75 to 140 GeV^2 at $\tau = 0.25$. On the basis of the deep inelastic results one would be surprised to find important scaling violations in such q^2 ranges.

5.2. Scaling in p production

A similar test of scaling has been performed by the CFS Collaboration with proton beams of 200, 300, and 400 GeV. In this analysis, scaling holds within 20%, but the same comment holds: scaling is tested in a q^2 range of 16 to 32 GeV^2 for the lowest $\tau = 0.04$ and of 80 to 160 for the highest $\tau = 0.2$.

We now have data obtained at the ISR corresponding to $\sqrt{s} = 62$ GeV. This enlarges very much the range of q^2 obtainable by comparing the spectrum shown in Fig. 2 with

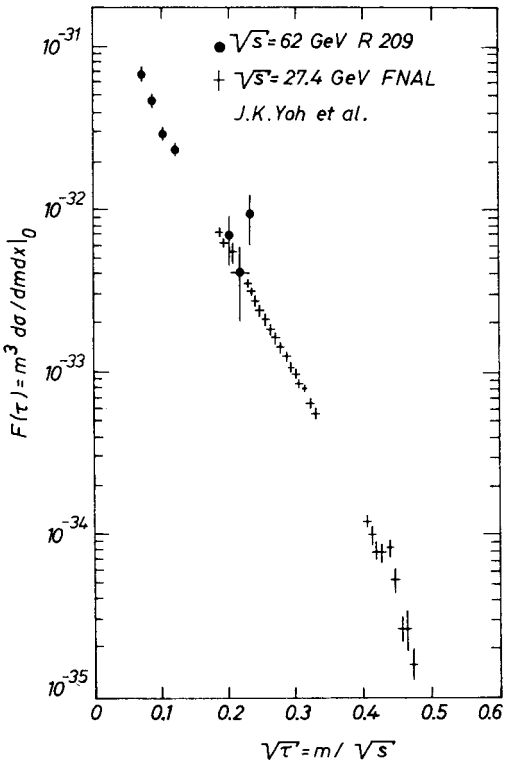

Fig. 10. $F(\tau) = m^3 d^2\sigma/dmdx|_{x=0}$

the FNAL result. But in practice the test is limited to the mass range between the resonances J/ψ and γ. This means that the ISR and FNAL results do not overlap in τ except in a very small region.

Figure 10 shows the quantity $m^3 d^2\sigma/dmdx|_{x=0} = F(\tau)$ as measured in the ISR and CFS experiments. The published data from FNAL are in terms of $d^2\sigma/dmdy$, where y is the rapidity

$$y = \tfrac{1}{2} \log \frac{E + P_L}{E - P_L}.$$

To convert the data one has to remember the formula:

$$\left.\frac{d^2\sigma}{dmdx}\right|_{x=0} = \frac{\sqrt{s}}{2m}\left.\frac{d^2\sigma}{dmdy}\right|_{y=0}.$$

Figure 10 emphasizes the unique contribution of the ISR, namely the possibility of mapping $F(\tau)$ for very small τ, but a test of scaling is limited to the region $\tau = 0.04$, which corresponds to the lower limit of the FNAL mass range and to the upper edge (a few events above the Υ) of the ISR mass range. This overlap shows that scaling holds within $\sim 50\%$ over a q^2 region extending now from 16 to 150 GeV^2. But this test is done at $x_F = 0$, namely $x_1 = x_2 = \sqrt{\tau} = 0.2$. Surprisingly this corresponds to the region where QCD predicts practically no scaling violation! But the lesson of the comparison is otherwise: $F(\tau)$ now measured from $\sqrt{\tau} = 0.05$ to $\sqrt{\tau} = 0.5$ extrapolates very smoothly from the region investigated at FNAL to the ISR region.

6. Extraction of quark structure functions

We have seen that, in the limit of the naïve Drell–Yan model the dimuon cross-section is related to the quark structure functions inside the nucleons. Parameters measured in deep inelastic lepton scattering (DIS) are also expressed in terms of quark structure functions.

If the idea of constituents is at all relevant, one would expect the distributions to be independent of the probe used to measure them. Actually this assumes the theoretical prejudice that structure functions determined for $q^2 < 0$ via the Drell–Yan model and for $Q^2 > 0$ via DIS are identical.

6.1. Pion structure function

This is a unique contribution of dilepton experiments, since it is very difficult to probe the pion constituents otherwise. The most complete analysis was performed in the NA3 experiment. The advantage of using a pion beam comes from the fact that pions have valence antiquarks and one can neglect the pion sea. Then the cross-section simplifies:

$$\frac{d^2\sigma}{dx_1dx_2} \propto \frac{1}{x_1^2x_2^2} V(x_1)G(x_2),$$

where x_1 and x_2 are extracted from the measurable quantities:

$$m^2 = x_1x_2s, \quad x_F = x_1 - x_2.$$

There is only one function for valence quarks inside the pion:

$$V(x_1) = \bar{u}_v^{\pi^-}(x_1) = d_v^{\pi^-}(x_1) = u_v^{\pi^+}(x_1) = \bar{d}_v^{\pi^+}(x_1).$$

The first test is to check that the cross-section expressed in terms of x_1 and x_2 factorizes in the form: function (x_1) × function (x_2). This test is not completely satisfactory, which could come from the neglect of the pion sea.

There is a way of eliminating the pion sea altogether by subtracting the π^- and π^+ cross-sections after proper normalization. It also completely eliminates the nucleon sea contribution.

In the case of a Pt target one finds:

$$\left(\frac{d^2\sigma}{dx_1 dx_2}\right)_{(\pi^- \mathrm{Pt})-(\pi^+ \mathrm{Pt})} \propto \frac{1}{x_1^2 x_2^2} V(x_1) \tfrac{1}{9} [u_v(x_2)+2d_v(x_2)],$$

where

$$u_v(x) = u^p(x) = d^n(x),$$

$$d_v(x) = d^p(x) = u^n(x).$$

The factorization method works better and one extracts the shape of the pion structure function shown in Fig. 11:

$$V(x) \propto x^{0.4\pm0.06}(1-x)^{0.9\pm0.06}.$$

This is a much flatter distribution than in the nucleon case. This analysis also gives the sea component of the pion and, by studying the function (x_2), the nucleon structure functions.

For the nucleon the results are as follows:

$$u_v(x) = 10.5x^{1.02}(1-x)^{4.04},$$

$$d_v(x) = 6.3x^{1.02}(1-x)^{5.04},$$

$$S(x) = 0.35(1-x)^{6.0}.$$

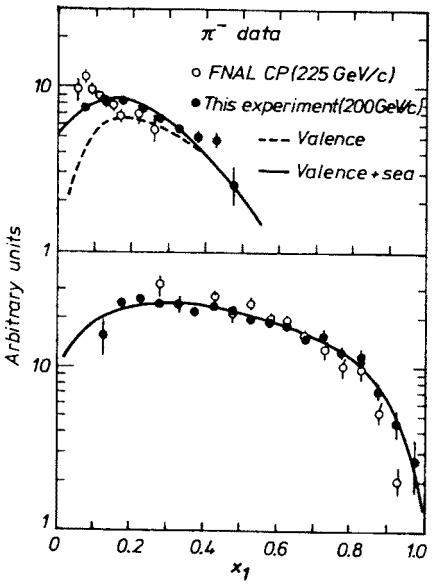

Fig. 11. Pion structure function

The shapes of the valence quark distributions agree well with those obtained in deep inelastic neutrino scattering (CDHS experiment) [11], but their integrals are about twice as high as in the case of the neutrino results. The sea contribution being small the sea structure function is not determined reliably, and other results will be presented later.

For the pion structure functions the integrals are very much consistent with general expectations:

$$2x \int V(x)dx = 0.34, \quad 6x \int S(x)dx = 0.10.$$

This is obtained with a number of colours $N_c = 3$. If one does not take a colour factor into account, the integrals become three times smaller, disagreeing with other experiments.

6.2. Proton structure function

In proton-induced reactions one has now a case of the valence × sea process. This explains the difficulty of the analysis, but also the interest of it, because of its high sensitivity to the sea component inside the nucleon. The pN reactions are also available in larger s ranges than πN reactions. In particular the ISR result gives data at very small τ, allowing the probing of the deeper sea. The NA3 experiment has also obtained data with a proton beam. This allows to extract the new nucleon structure functions:

$$u_v(x) = 2.25\sqrt{x}\,(1-x)^{3.2},$$

$$d_v(x) = 1.26\sqrt{x}\,(1-x)^{4.2},$$

$$\bar{u}(x) = \bar{d}(x) = 0.37(1-x)^{9.4},$$

$$\bar{s}(x) = \tfrac{1}{4}(\bar{u}(x)+\bar{d}(x)).$$

These structures functions are different from the ones extracted in the π-N data; in particular the sea becomes now much steeper than before. As a test we can try both sets of structure functions in the interpretation of results obtained by other experiments.

From the basic Drell–Yan formula one obtains:

$$\sum_i e_i^2[f_i(x_1)\bar{f}_i(x_2)+\bar{f}_i(x_1)f_i(x_2)]\delta(\tau-x_1x_2) = \frac{m^3 d^2\sigma/dmdx_F}{(8\pi\alpha^2/3N_c)\,(1/\sqrt{x_F^2+4\tau})}.$$

Experimentally, data exist essentially for $y = x_F = 0$. This corresponds to $x_1 = x_2 = \sqrt{\tau}$. One then extracts

$$\sum_i e_i^2 f_i(\sqrt{\tau})\bar{f}_i(\sqrt{\tau}) = A,$$

where

$$A = m^3 \frac{d^2\sigma}{dmdx_F}\bigg|_{x_F=0} \frac{3N_c\sqrt{\tau}}{8\pi\alpha^2}.$$

Remembering that 1 cm × GeV = $10^{13}/0.197$ one gets the totally dimensionless quantity A plotted in Fig. 12, based on ISR and CFS data.

One can now develop A in terms of structure functions

$$A = \tfrac{4}{9} u\bar{u} + \tfrac{1}{9} d\bar{d} + \tfrac{1}{9} s\bar{s} + \ldots$$
$$= \tfrac{4}{9} (u_v + u_s)\bar{u}_s + \tfrac{1}{9} (d_v + d_s)\bar{d}_s + \tfrac{1}{9} s\bar{s} + \ldots .$$

There are too many variables to extract from one experimental curve! But we can test the consistency of these results with the structure functions obtained in the NA3 experiment just described. The result for the quantity A is shown on Fig. 12. When one

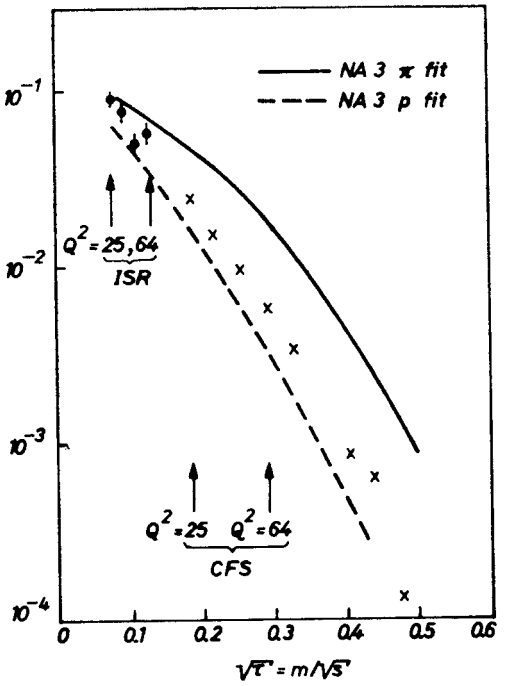

Fig. 12. $A = \Sigma e_i^2 f(x)\bar{f}(x)$ with fits using two different sets of structure functions

uses the NA3 structure functions extracted from the π–N data, the discrepancy with the experimental points is very large. It is not only an over-all different normalization: the data request a steeper slope. This can be achieved by using a steeper distribution for the sea. Indeed when one uses the NA3 structure functions extracted from the p–N data, the experimental points are much better fitted in slope over a large $\sqrt{\tau}$ range. The normalization problem will be discussed later.

This second analysis has assumed an almost SU(3) symmetric sea, namely $\bar{u} = \bar{d}$ and $\bar{s} = \frac{1}{4}(\bar{u} + \bar{d})$. It is tempting to go beyond this restriction and also to consider more than three quarks. Some hints have been given [1] that the $\bar{u}$ sea may be steeper than the $\bar{d}$. A complete analysis of quark structure functions inside the nucleon has still to come, with the various inputs from ν, e and μ scattering, and from Drell–Yan processes especially dimuon production in $\bar{p}$-induced reactions.

7. QCD corrections to the Drell–Yan model

7.1. Dilepton transverse momentum

This is where the naïve model conflicts the most with experiment. As a consequence this gives the most direct test for QCD corrections. In the basic model the dimuon transverse momentum p_T is the sum of the transverse momenta of the annihilating quarks. Because

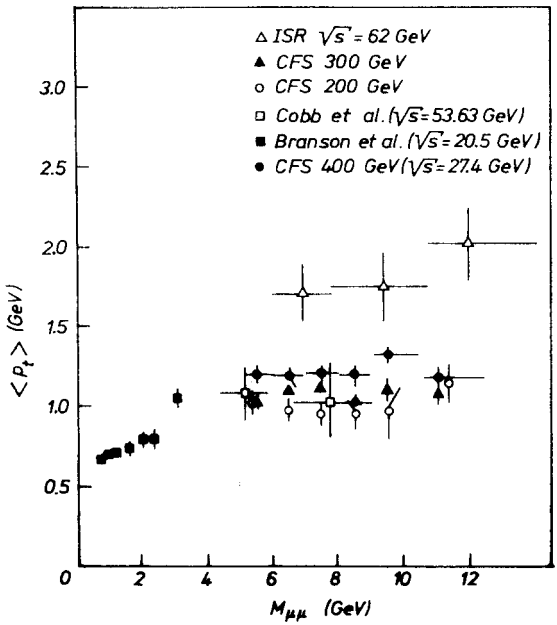

Fig. 13. $\langle p_T \rangle$ distribution for various energies

of confinement one expects an intrinsic quark k_T of order 300 MeV/c independent of the beam energy. This gives a dilepton p_T of order 500 MeV/c. The data in pN differ from expectation in two ways:

(*i*) $\langle p_T \rangle$ increases with the dimuon mass up to a mass of 4 GeV and then reaches a plateau.

(*ii*) The plateau value increases with s, possibly as fast as s. This is shown in Fig. 13, with data from the CFS 200, 300 and 400 GeV beams, and the ISR experiment at $\sqrt{s} = 62$ GeV. The increase of p_T can be parametrized:

$$\langle p_T \rangle = (600 + 22\sqrt{s})\ \text{MeV}/c.$$

Qualitatively one can understand the origin of the large $\langle p_T \rangle$ phenomenon in the higher-order diagrams of Fig. 4, where the high dilepton $\langle p_T \rangle$ is balanced by, for instance, a gluon jet. In fact QCD predicts a growth [8]:

$$\langle p_T^2 \rangle \propto \alpha_s q^2 + \text{const.}$$

and one can think of the constant term as coming from an intrinsic quark transverse mo-

mentum. On the other hand, p_T does not seem to depend on x_F. Results in π^--induced events show similar trends, with the interesting result that $\langle p_T \rangle$ is higher in π^- reactions than in proton reactions at the same energy.

7.2. The K factor

It has already been mentioned that, although the shapes of structure functions obtained in Drell–Yan and in neutrino DIS agree, the integrals seem to differ. The NA3 collaboration has done a systematic study of this effect. It compared the experimental results with the Drell–Yan prediction implemented with measured structure functions. These functions are normalized such that they reproduce the correct number of quarks in the nucleon.

The comparison has been done with incident pions, protons and antiprotons. In all cases it is found that the data lie more than a factor 2 (K factor) above the prediction. The

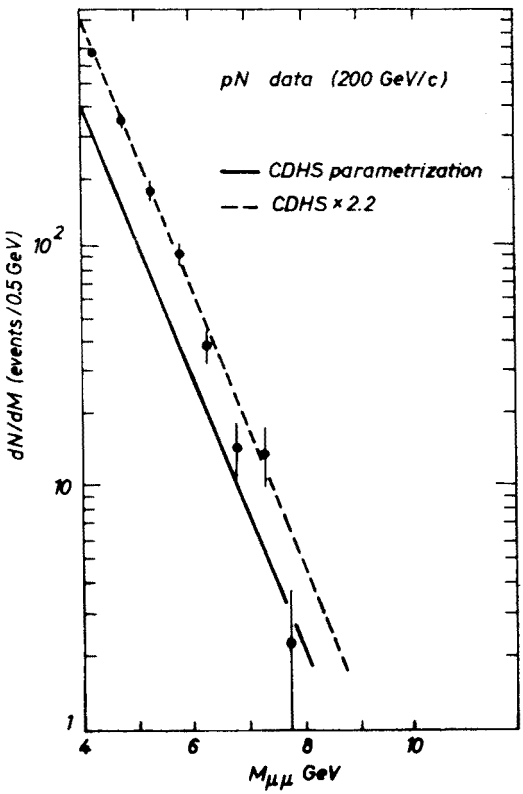

Fig. 14. The K factor in the pN data from the NA3 experiment

example of the p-N reaction is shown in Fig. 14. This could be the first evidence for a multiplicative correction factor coming from QCD effects as anticipated in the educated model.

With the ISR result the conclusion is not so straightforward. Fig. 15 shows the mass spectrum compared with the Drell–Yan prediction when using the NA3 and the CDHS

structure functions. The two sets of functions give similar results for large dimuon masses ($x > 0.2$) in an x range where they have indeed been measured. Here the data could accomodate a factor $K \simeq 2$. In the low mass region ($0.06 < x < 0.12$) the two sets give somewhat different expectations. With the NA3 structure functions the data is only ~20% above

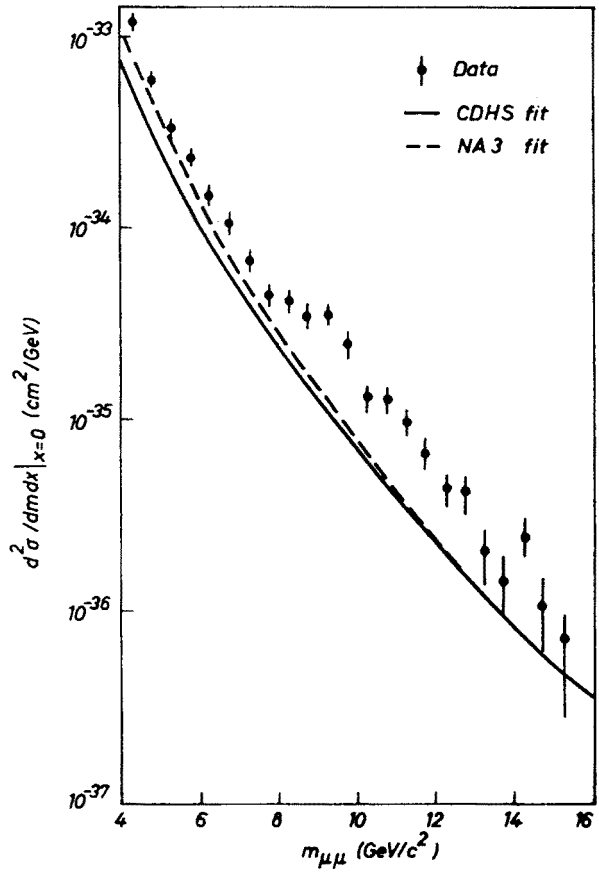

Fig. 15. The K factor in the ISR experiment with NA3 and CDHS structure functions

the prediction, while with the CDHS structure functions we need a factor $K \simeq 1.7$. Both NA3 and CDHS experiments measure the structure functions for $x > .2$ and the extrapolation to small x has no reason to be valid.

8. Associated hadrons

As already discussed, the ISR experiment is able to look at charged hadrons associated with the dimuons. The inner detector is located in a space without magnetic field and this means that the only information available will be on multiplicity and directionality.

The total multiplicity of charged hadrons decreases with the energy carried away by the dimuon. More interesting is the evolution of multiplicity with the dimuon $\langle p_T \rangle$.

The multiplicity seen in the hemisphere towards the dimuon system stays constant. On the contrary, the multiplicity seen in the hemisphere away from the dimuon system increases with $\langle p_T \rangle$. This is shown in Fig. 16. This feature is expected in a model where the high $\langle p_T \rangle$ dimuon is balanced by a jet as in some graphs of Fig. 4.

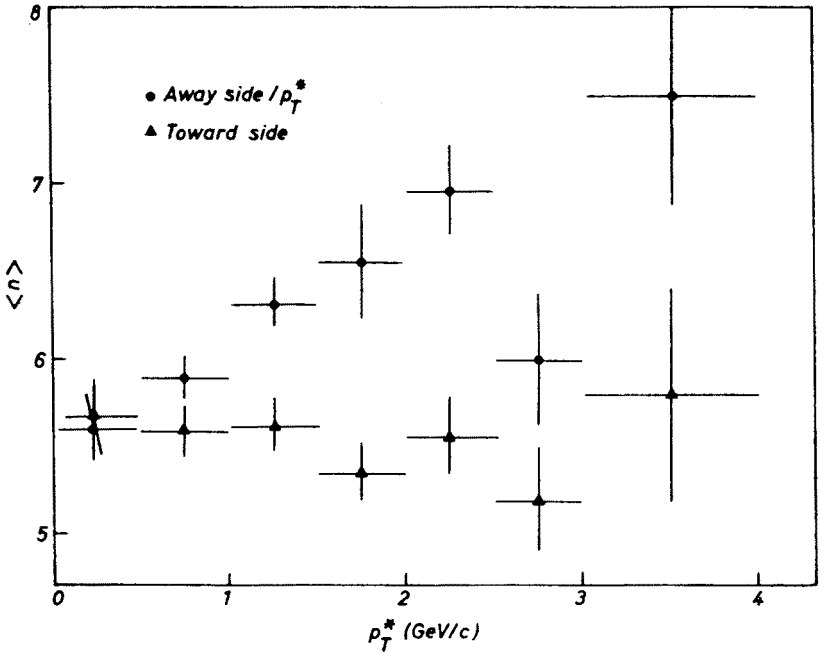

Fig. 16. Hadron multiplicity associated with the dimuon $\langle p_T \rangle$

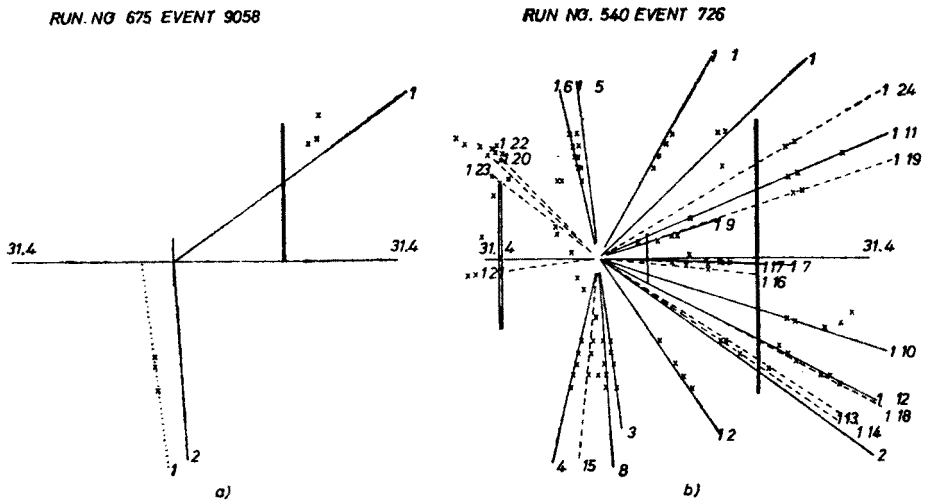

Fig. 17. Display of events in the inner detector (a) without and (b) with accompanying hadrons

Finally there is a class of events of special interest: they do not show any hadrons accompanying the two muons in the inner detector. Such an event is shown in Fig. 17a, while a normal event is seen in Fig. 17b. The number of events with zero hadrons ($\sim 1\,\%$ of all events) is larger than the number of events with one hadron. This gives a break in the

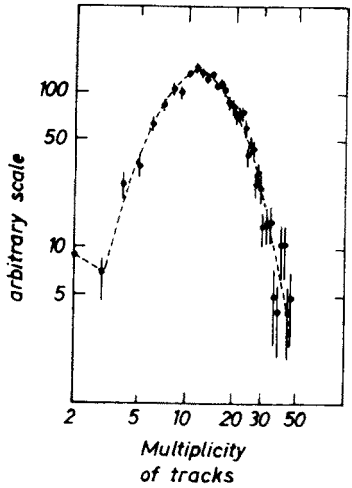

Fig. 18. Multiplicity of tracks reconstructed in the IRS vertex detector

multiplicity distribution and points to a new mechanism of dimuon production. This is clearly shown on Fig. 18.

The kinematics of the ~ 100 events produced without hadrons has been studied. The events reconstruct low masses, their $\langle p_T \rangle$ is lower than for normal dimuon events, and

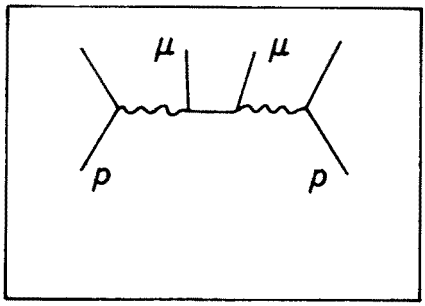

Fig. 19. Diagram of the two-photon process in pp reaction

they tend to be coplanar. These characteristics point toward the possibility of the two-photon mechanism. The elastic part of this process is represented by the diagram of Fig. 19. It has been studied some time ago [14]. A large part of it goes through the elastic channel

$$pp \rightarrow pp\mu^+\mu^-$$

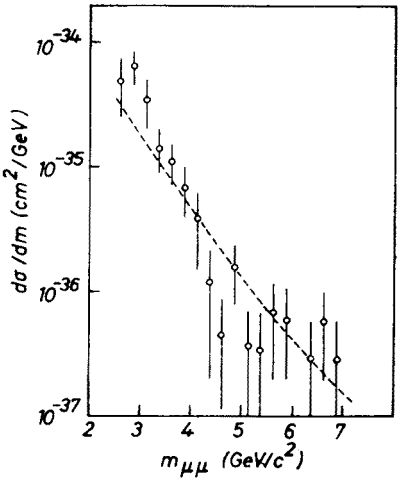

Fig. 20. Cross-section of the two-photon process at the ISR. The dashed line represents the elastic contribution only

explaining why no hadrons are seen in the vertex detector. Furthermore the cross-section anticipated [15] is in good agreement with the experimental result as seen in Fig. 20.

Thus this category of events seems to give the first evidence for a two-photon process in pp reactions. This process still very small compared with the dominant Drell–Yan contribution at ISR energies (1 %) increases rapidly with s and should become substantial at the newly built $p\bar{p}$ collider or Isabelle machine.

9. *Conclusions*

We have seen the striking qualitative successes of the Drell–Yan model. This gives a new support for the idea of hadron constituents with quark quantum numbers. We have also seen that it is necessary to go beyond the naïve model, and the topic of dilepton production is becoming a very useful laboratory for QCD computations. On the other hand, these QCD effects affect only very small kinematical regions, or give an over-all renormalization, and this explains why the predictions of the simple model are well satisfied for the majority of the data.

Many new experimental results have been found in the last three years, keeping dilepton physics very lively, and giving us a satisfactory understanding of the process.

Progress will come with more statistics. But the cross-sections fall dramatically fast and an order of magnitude gain in statistics only extends the mass range by 2 to 3 GeV. Thus it will not be surprising if progress goes at a slower pace, now that the foundations are firmly laid.

REFERENCES

[1] J. K. Yoh et al., *Phys. Rev. Lett.* **41**, 684 (1978); **41**, 1083 (1978); D. M. Kaplan et al., *Phys. Rev. Lett.* **40**, 435 (1978); L. M. Lederman, Proc. 19th Int. Conf. on High-Energy Physics, Tokyo 1978 (*Phys. Soc. Japan*, Tokyo 1979), p. 706.

[2] D. Antreasyan et al., preprint CERN-EP/79–116, presented at the EPS Int. Conf. on High--Energy Physics, Geneva, July 1979.
[3] C. B. Newman et al., *Phys. Rev. Lett.* **42**, 951 (1979); G. E. Hogan et al., *Phys. Rev. Lett.* **42**, 948 (1979); K. J. Anderson et al., *Phys. Rev. Lett.* **42**, 944 (1979).
[4] J. Badier et al., preprints CERN-EP/79–61 (1979) and CERN-EP/79–68 (1979).
[5] M. A. Abolins et al., preprint CERN-EP/79–69 (1979).
[6] S. D. Drell, T. M. Yan, *Phys. Rev. Lett.* **25**, 316 (1970).
[7] See for instance E. L. Berger, preprint SLAC-PUB 2314 (1979).
[8] G. Altarelli, Kupari-Dubrovnik Summer School, September 1979.
[9] J. G. Branson et al., *Phys. Rev. Lett.* **38**, 457 (1977).
[10] E. L. Berger, S. J. Brodsky, preprint SLAC-PUB 2247 (1979).
[11] J. G. H. de Groot et al., *Z. Phys.* **1**, 143 (1979).
[12] Rencontre de Moriond, March 1980
[13] J. Badier et al., CERN/EP 79–147.
[14] M. S. Chen, *Phys. Rev.* **D7**, 3485 (1973).
[15] Calculation done at CERN by J. A. M. Vermaseren.